Turkish Journal of Chemistry

http://journals.tubitak.gov.tr/chem/

Research Article

Turk J Chem
(2016) 40: 28 – 37

doi:10.3906/kim-1407-7

Characterization and photocatalytic properties of TiO_2/chitosan nanocomposites synthesized by hydrothermal process

Funda SAYILKAN[1,2,*], **Fatma Bilge EMRE**[1,2]

[1]Prof. Dr. Hikmet Sayılkan Advanced Materials Research and Application Laboratory, Scientific and Technological Research Center, İnönü University, Malatya, Turkey

[2]Department of Elementary Education, Faculty of Education, İnönü University, Malatya, Turkey

Received: 03.07.2014 • **Accepted/Published Online:** 05.04.2015 • **Final Version:** 05.01.2016

Abstract: Nanocomposites of TiO_2/chitosan (nTC) were synthesized by hydrothermal process at 200 °C. Photocatalytic activity of the nanocomposites was studied with degradation of malachite green (MG) in aqueous medium. Structural and physico-chemical properties of the obtained nanocomposites were characterized by XRD, SEM, BET, FTIR, and particle size analyzer. Complete photodegradation of MG was successfully achieved with the aid of the nanocomposites. The optimum photocatalytic degradation conditions, irradiation time, irradiation power, and amount of catalyst were studied. Photocatalytic activity of the synthesized nanocomposites in terms of degradation of MG was compared with that of undoped TiO_2 (synthesized by our team) and chitosan under normal conditions. It was concluded that the synthesized nanocomposites had better photocatalytic activity. The best result (100% degradation) was obtained with amount of nTC of 0.25 g and irradiation time of 120 min.

Key words: Nanocomposite, photocatalytic activity, photodegradation, hydrothermal process

1. Introduction

Chitosan is a linear, semicrystalline polysaccharide composed of β-(1-4)-linked-D-glucosamine and N-acetil-D-glucosamine units.[1] The structure of this polymer is explained in Figure 1.

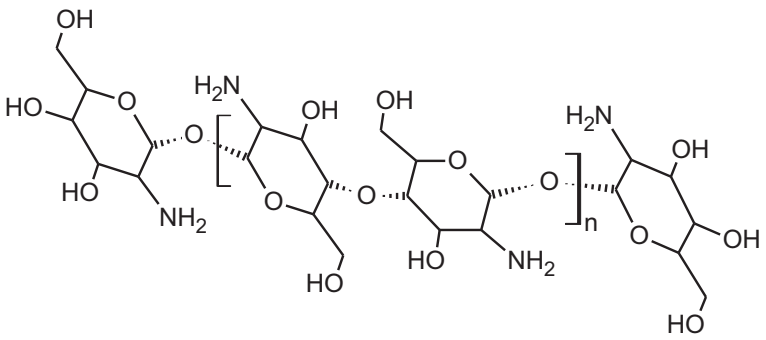

Figure 1. Structure of chitosan.

Due to the specific features of these amino groups, chitosan also efficiently forms complexes of various species such as metal ions, and therefore they are often used for the treatment of wastewaters, by purifying

*Correspondence: funda.gurer@inonu.edu.tr

them through removing heavy metals.[1] The complex ability of chitosan is further utilized to refine beverages (wine, juices, etc.).[2] Moreover, chitosan exhibits other remarkable intrinsic properties: this polysaccharide exhibits antibacterial activity,[3,4] along with antifungal[5] and mucoadhesive.[6] It can be biodegraded into nontoxic residues[7,8]—the rate of its degradation is highly related to the molecular mass of the polymer and its deacetylation degree—and its biocompatibility with physiological medium has been proven to some extent.[9,10] All these singular features make chitosan an outstanding material for biomedical applications.[11]

TiO_2 is one of the most commonly used photocatalysts for degradation of pollutants.[12–16] As it is environmentally friendly, cheap, nonphotocorrosive, stable, highly available, and capable of mineralizing pollutants completely, it has been largely used as the catalyzer for water decontamination.[17,18] Nano-TiO_2 and its composites can be synthesized by different methods such as sol-gel and hydrothermal method.[19,20] Hydrothermal synthesis is a nanoparticle preparation route that utilizes heat and pressure to initiate reactions of reagents dissolved in water or organic solvent. Nanoparticles can be produced without the requirement for postreaction calcinations. The method is attractive as it can produce nanoparticles and nanocomposites with minimal or no agglomeration.[19,21]

In recent years, chitosan biopolymer (CS) has shown multifunctional performance with TiO_2 in heterogeneous photocatalysis technology, including its use as a stabilizer,[22] a recovery agent[23] for increasing the adsorption capacity of CS-TiO_2 adsorbent in the removal of metal ions,[24,25] and for enhancing the adsorption–photocatalytic process of dye and organic pollutant species.[25–29]

Malachite green (triphenylmethane dye) (MG) is a basic cationic dye readily soluble in water. MG is widely used for coloring leather and silk and it is well known as an effective, inexpensive topical fungicide and disinfectant used in the aquaculture industry. However, the toxic effects of MG have been studied extensively.[30,31] Therefore, different methods (adsorbtion,[32] photocatalysis,[33] sonosorption[34] etc.) were used to remove MG from wastewater.

The aim of the present study was to demonstrate, unlike the previously reported studies (in situ sol-gel process,[35] coating[26] etc.), that TiO_2/chitosan nanocomposites were synthesized by a hydrothermal method using metal alkoxide. In this method, experiments were performed at relatively low temperature and short experiment time. New materials were used for the photocatalytic degradation of MG dye. Overall the experiment showed that the new nanocomposites are good for photocatalytic degradation of MG, which is a hazardous dye.

2. Results and discussion

2.1. Characterization of the nanocomposites

The crystalline structure of the synthesized nanocomposites was analyzed by XRD. When the XRD pattern of the nanocomposites (Figure 2) was compared with PDF#21-1272 data files, it was found that all of the sharp peaks belong to anatase phases. XRD patterns of the nanocomposites, pure TiO_2, and chitosan are demonstrated in Figure 2. According to the calculations performed by using the Scherrer equation,[36] average crystallite size of the nTC and undoped TiO_2[37] was 11.8 nm and 8 nm, respectively.

Some of the physicochemical properties of the synthesized nTC are given in Table. The BET surface area, average pore diameter, and micropore volume of the nanocomposites were calculated from the N_2 adsorption isotherm obtained at liquid N_2 temperature, where the sample was degassed at 130 °C for 4 h before N_2 adsorption. It was found that the BET surface area, average pore diameter, and micropore volume were 174

m^2/g, 8.70 nm, and 0.033 mL/g, respectively. According to the result of the DFT plus method, mesoporosity dominated and was distributed in the range of 5–20 Á. The mesoporosity (ratio of mesopores to total pore volume, Vme/Vtot) was 98.1%. The microporosity (ratio of micropores to total pore volume, Vmi/Vtot) was 1.9%.

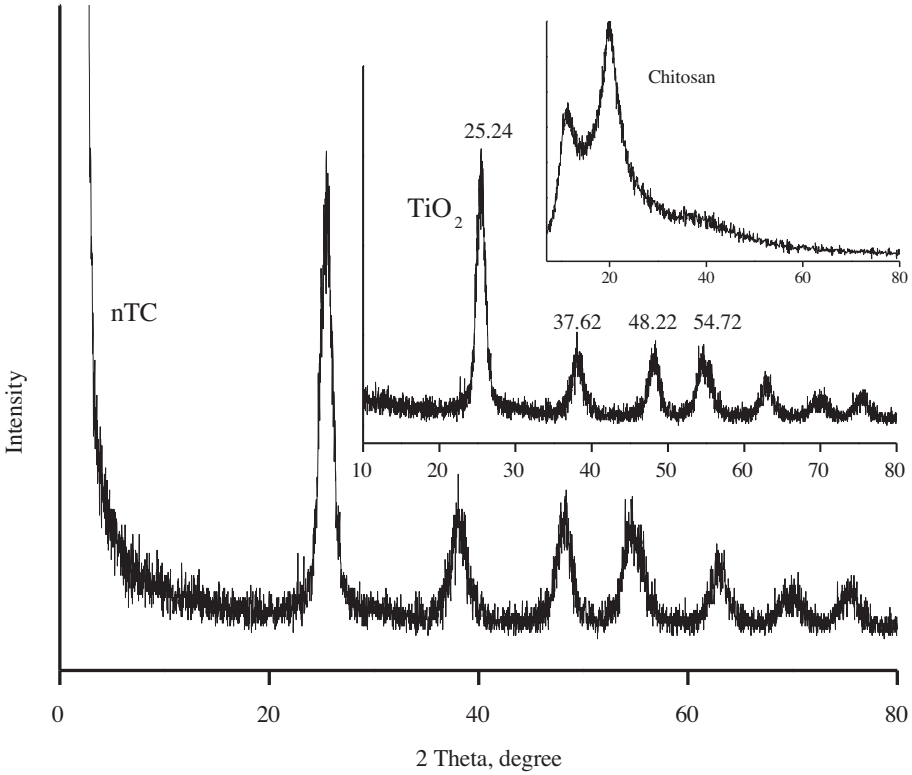

Figure 2. The XRD patterns of nTC, pure TiO_2,[37] and chitosan.

Table. Some physicochemical characteristics of the synthesized nTC and comparison with the literature (NR: not reported).

Crystalline type	Crystalline size (nm)	BET surface area (m^2/g)	Average pore diameter (nm)	Micropore volume (mL/g)	Particle size (nm)	Degradation (%)	Reference
Anatase/ Brookite	NR	3.8	15.24	0.043	NR	41–91	[25]
Anatase/ Rutile	4–18	NR	NR	NR	NR	87 (max)	[26]
NR	NR	1.342				90	[27]
Anatase	11.8	174	8.70	0.033	168	100	This study

The functional group of the hydrothermally synthesized nanocomposite was analyzed by FT-IR (Figure 3). Both TiO_2 and nTC were observed through the main bands due to stretching vibrations of OH groups between the range of 3600 cm^{-1} and 3000 cm^{-1}. The vibrations of amine group NH_2 (ν = 1535 cm^{-1}) and the vibrations of the hydrogen bond and protonation of the amino groups (ν = 1410 cm^{-1}) were observed in the composite (nTC).[38] Vibration frequencies related to the C–H bonding –CH_2 (ν = 2930 cm^{-1}) and –CH_3

(ν = 2980 cm^{-1}) were observed. Bending vibrations of methylene and methyl groups were also visible at 1380 cm^{-1} and 1460 cm^{-1}, respectively.[39] Moreover, characteristic peaks related to TiO_2–TiO_2 (Ti–O/Ti–O–C) (ν = 1000–1200 cm^{-1}) were not observed in the nTC.

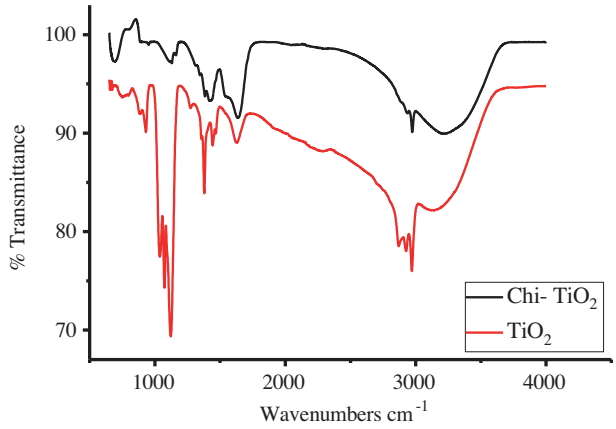

Figure 3. Typical FT-IR spectrum of pure TiO_2 and synthesized nTC particles.

Typical SEM images of nTC particles and pure TiO_2[37] are shown in Figure 4. This figure indicates that the shapes of the particles are quite similar to each other and they are likely to become spherical.

Particle size of nanocomposites was determined by particle size analyzer. The particle size distribution of the nTC is shown in Figure 5.

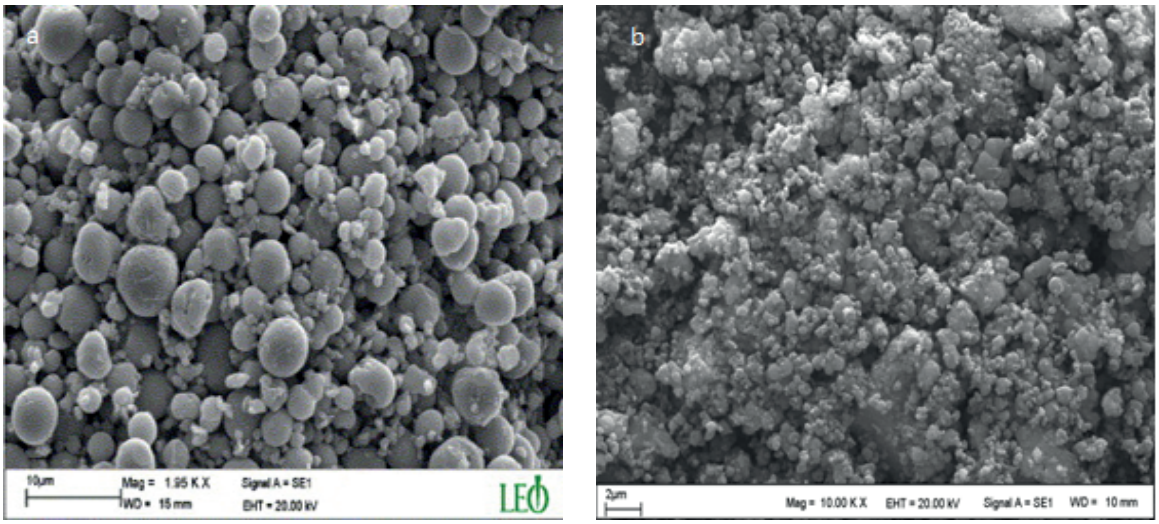

Figure 4. Typical SEM microphotograph of hydrothermally synthesized a) pure-TiO_2[37] and b) nTC particles.

2.2. Photocatalytic degradation of MG

The strong preadsorption of the MG on the nTC surface is an important phenomenon for an efficient charge transfer, and it not only affects the photodegradation rate, but also changes the photocatalytic mechanism. For this reason, before examining the photocatalytic activity of nTC as a catalyst for degradation of MG, adsorption tests were carried out by keeping it at its natural pH, and containing MG (C_0 = 30 mg/L, 25 mL) and 0.25 g

of nTC in the dark at room temperature for 30, 60, 90, and 120 min. It was determined that the adsorption process on nTC was completed after 120 min and the adsorption at 614 nm (λ_{max}) did not change with the prolonged soaking time from 90 to 120 min. Therefore, before the optimization studies nTC/MG mixtures were kept in the dark for 90 min.

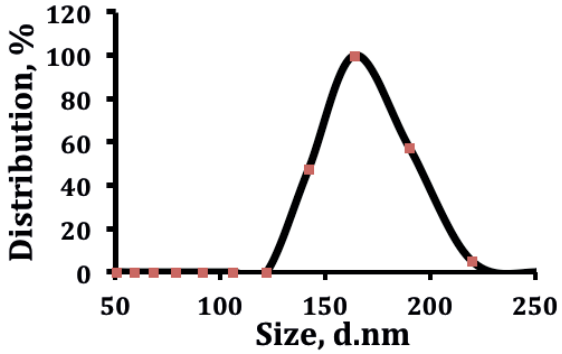

Figure 5. Particle size distribution of nTC.

The photocatalytic degradation of MG was examined by using the hydrothermally synthesized nTC crystalline as catalyst under irradiation. Photocatalytic degradation of MG catalyzed by nTC under different irradiation times is shown in Figure 6a. Normalized concentration variations with irradiation power, amount of nTC, and initial MG concentration in the mixture are also shown in Figures 6b–6e, respectively.

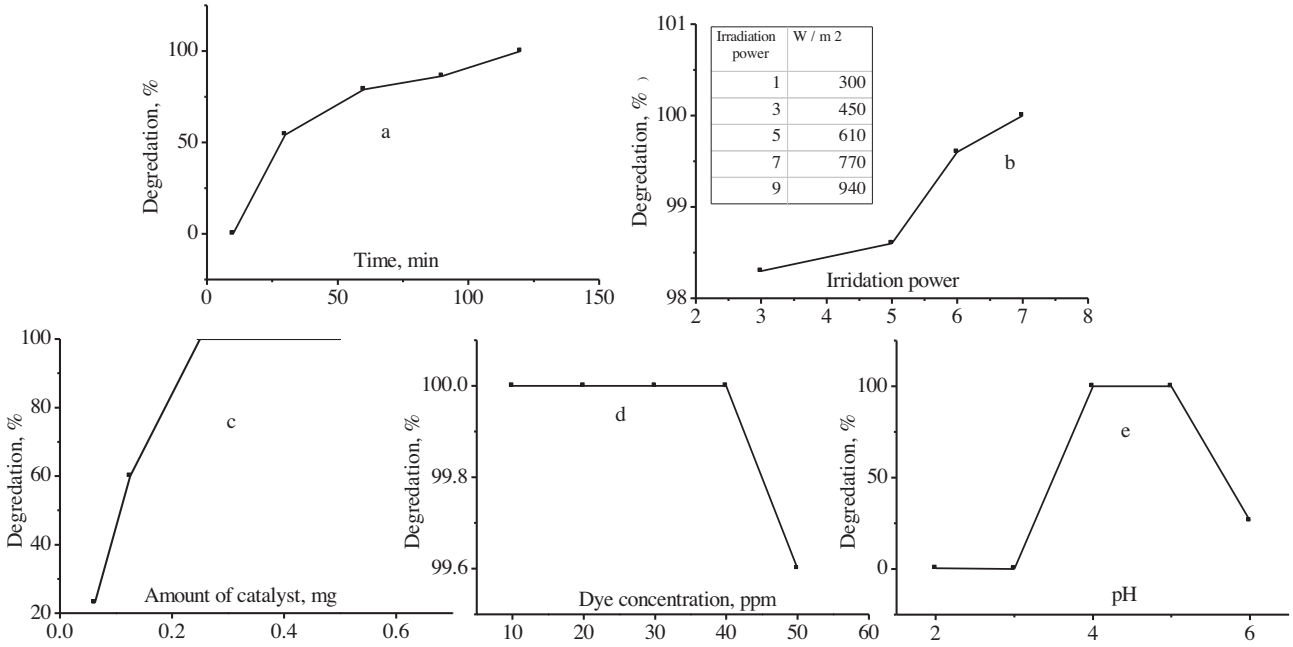

Figure 6. Photocatalytic degradation of MG a) Effect of irradiation time, b) Effect of irradiation power, c) Effect of amount of catalyst, d) Effect of dye concentration, e) Effect of pH.

The effects of irradiation time on the degradation of MG at constant irradiation power (770 W/m^2, PI 7), amount of the nTC (0.25 g), initial concentration of dye (30 mg/L, 25 mL), and in natural pH were examined.

The effect of irradiation time on MG degradation is shown in Figure 6a. The increase in irradiation time made the nTC/MG mixture colorless, which indicated the degradation of MG. Decolorization was completed at 120 min for nTC. Generally, the logarithmic plot of concentration data gives a straight line, the slope of which helps to predict the rate constant of the reaction. That is $\ln C_0/C = kt$, where C is the dye concentration (mg/L) at instant t (min), C_0 is the dye concentration (mg/L) at t = 0 (min), and k is a rate constant (1/min). The first order rate constant k was obtained from the slope of the linear plot of $\ln(C_0/C)$ versus time. Figure 7 shows that $\ln(C_0/C)$ is linear with the irradiation time, obtained by replotting in the $\ln(C_0/C)$-t coordinates; this means that photodecomposition of MG obeys the rules of pseudo-first order reaction kinetics. The reaction rate decreases with irradiation time since it follows apparent first-order kinetics and additionally competition for degradation may occur between the reactant and the intermediate products. The difficulty of converting the N-atoms of dye into oxidized nitrogen compounds causes slow kinetics of dye degradation after a certain time limit. The deactivation of active sites by strong by-products deposition (carbon, etc.) causes a reaction of short chain aliphatic with OH· radicals and the short life-time of photocatalyst.[37,40]

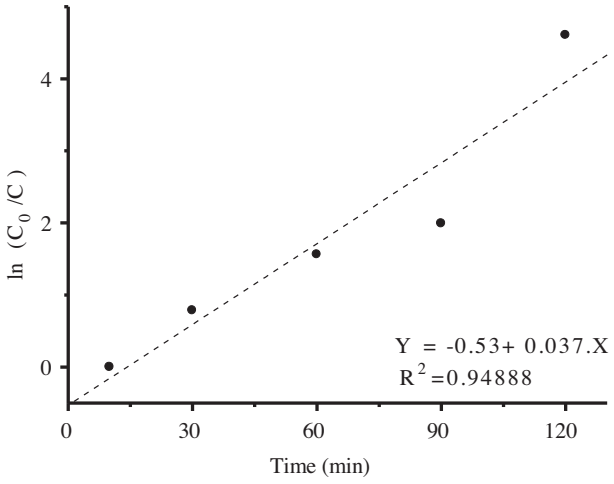

Figure 7. Pseudo-first-order photodegradation kinetics of MG.

The effects of irradiation power on the degradation of MG at constant irradiation time (120 min), amount of the nTC (0.25 g), initial concentration of dye (30 mg/L, 25 mL), and in natural pH were examined. The results are presented in Figure 6b. It can be seen that MG completely degrades with increasing irradiation power up to 770 W/m^2. The mixture became transparent and colorless, suggesting that degradation at these levels results in complete mineralization.[41,42] This is probably due to the fact that low light intensity reactions involving electron–hole (e^-/h^+) formation are predominant and electron–hole recombination is negligible. However, as the light intensity increased, so did the light electron–hole recombination, which caused the reaction rate to decrease.

To optimize the amount of catalyst, a series of experiments were carried out in which the loading varied from 0.1 to 0.5 g with a dye concentration of 30 mg/L, irradiation power 770 W/m^2, irradiation time 120 min, and in natural pH. The degradation efficiency of MG for various catalyst loadings is shown in Figure 6c. The results indicate that the photocatalytic efficiency increases up to a maximum as a function of catalyst loading. The optimum amount of catalyst was determined as 0.25 g. The increased amount of catalyst produces a proportional increase in the number of active radicals by absorbing increased numbers of photons, which are sufficient and readily accessible for the degradation of nearby MG.[43,44]

The photocatalytic degradation at different initial concentrations of MG in the range of 10–50 mg/L was examined with determined conditions as the irradiation time (120 min), irradiation power (770 W/m^2), amount of the nTC (0.25 g), and in natural pH. As shown in Figure 6d, the photocatalytic degradation efficiency of MG by nTC under the UV-light decreased with increases in the concentration of MG. This negative effect can be explained as follows: as the dye concentration increases, the equilibrium adsorption of dye on the catalyst surface active sites increases too; hence competitive adsorption of O_2 on the same sites decreases, meaning a lower formation rate of $O_2\bullet^-$, H_2O_2, and $\bullet OH$ radical, which is the principal oxidant necessary for high degradation efficiency. On the other hand, when the Beer–Lambert law is taken into account, as the initial dye concentration increases, the path length of photons entering the solution decreases, which results in lower photon adsorption on catalyst particles and, consequently, a lower photodegradation rate.[45–47]

Several tests were performed to observe the effect of pH on photodegradation in the determined conditions (Figure 6e). Natural pH of the nTC/MG mixture (containing 0.25 g of nTC and 30 mg/L MG) was nearly 4. pH of the medium varied between 2 and 6 by addition of HCl and NaOH. It was found that the highest degradation activity was observed at pH 3 and pH 4. Above and below this pH value activities decreased. This behavior shows that the interaction between catalyst and dye must occur because of the interaction of acid sites MOH_2^+ or amphoteric sites MOH of catalysts with amine or aromatic groups of MG dye.[48]

Photocatalytic activity of the synthesized nanocomposites for degradation of MG was compared with undoped-TiO_2[37] and chitosan at optimum conditions. Photocatalytic degradation results for nTC, undoped TiO_2, and chitosan were 100%, 90%, and 88%, respectively. This result shows that nanocomposites (nTC) had the best photocatalytic activity. The photocatalytic mechanism of MG is represented in Figure 8.

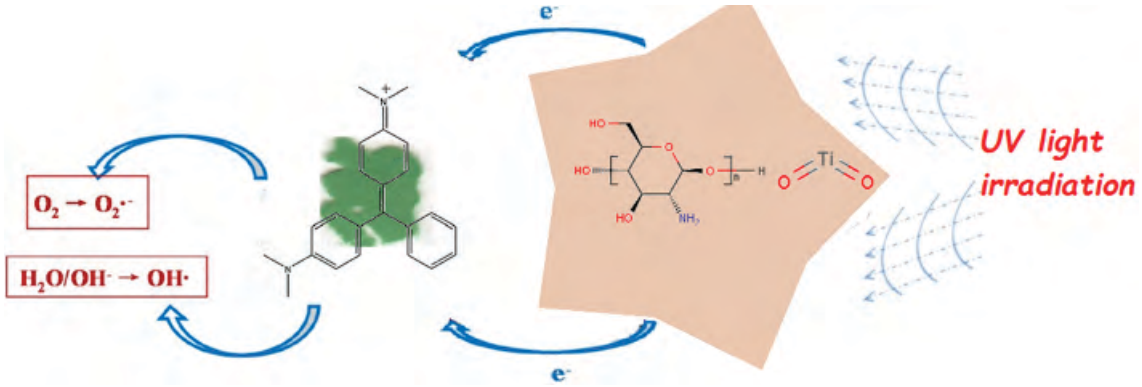

Figure 8. Possible photocatalytic degradation mechanism of MG.

In this study, nanocomposites (nTC) were easily synthesized by hydrothermal process at 200 °C in 4 h. This is a new method for synthesis of nTC. The synthesis of the new composite's structure was explained by analysis (FT-IR, XRD etc.). Afterwards, nTC was used for MG photocatalytic degradation. A possible degradation mechanism is demonstrated in Figure 8. Photocatalytic activity of the synthesized nanocomposites for degradation of MG was compared with that of undoped-TiO_2 and chitosan under optimum conditions. It was found that the synthesized nanocomposites had better photocatalytic activity. Results of this work were compared with the literature and summarized in the Table.

3. Experimental

3.1. Chemicals and apparatus

Tetraisopropylorthotitanate ($(Ti(OPr^i)_4$) (97%) and chitosan (MW = 100,000–300,000) provided by Alfa Aesar and Acros Organics, respectively, were used in the synthesis of nanocomposites to be used as photocatalyst. Acetic acid from Merck (HAc, 99%–100%) was used as solvent for chitosan. Isopropyl alcohol (Riedel de Haen, 99%) was used as solvent. Malachite green oxalate (MGO) purchased from a local textile factory was of analytical reagent grade and it was used without further purification. Deionized water was used for the hydrolysis of $Ti(OPr^i)_4$.

The crystalline structure of the nanocomposites was analyzed by X-ray powder diffraction (XRD) pattern obtained from Rigaku Geigerflex D Max/B diffractometer with Cu Kα radiation (λ= 0.15418 nm with a step of 0.04°). The crystallite size of the anatase particle was calculated using the Scherrer equation. Surface morphology of the nanocomposites was performed using SEM (LEO EVO 40). An ASAP 2000 model BET analyzer was used to determine the surface area and average pore diameter. The BET surface area, average pore diameter, and micropore volume of the nanocomposites were calculated from the N_2 adsorption isotherm at liquid N_2 temperature. The sample was degassed at 130 °C for 4 h before N_2 adsorption. Pore size distribution of the nanocomposites was computed by DFT plus method. FT-IR spectra were collected using a PerkinElmer Spectrum One FT-IR spectrometer. FT-IR measurements of the samples were carried out in transmission mode in the region from 700 cm^{-1} to 4000 cm^{-1} with ATR unit. Particle size of nanocomposites was determined by using a Malvern Nanoseries Zetasizer. Dye concentration in the solutions and mixtures was determined by using a Varian Cary 50 model UV/VIS spectrophotometer. Irradiation was carried out using a SOLARBOX 1500 model simulated irradiation unit with a Xe-lamp and a controller to change the irradiation time and power input from 390 to 1100 W/m^2.

3.2. Preparation of nanocomposites

Different amounts of chitosan (0.1, 0.2, 0.3, and 0.4 g) were added to alkoxide solution (5 g). The best photocatalytic degradation result obtained with the weight ratio of chitosan/$Ti(OPr^i)_4$ was 0.2/5 g/g. $Ti(OPr^i)_4$ was dissolved in i-propanol and chitosan (0.2 g) that was dissolved in 3% HAc. The preparation was stirred at ambient temperature for 10 min until it became homogeneous. Chitosan/HAc mixture was added dropwise to the alkoxide solution quickly. The hydrolysis reaction started at this step. After being stirred for about 30 min, the solution was transferred into a stainless steel Teflon-lined autoclave and heated at 200 °C for 4 h and the condensation reaction of the mixture was completed. Then the powders, which had been separated through centrifuging, were dried in a vacuum sterilizer at 40 °C for 4 h. In this way, the nanocomposite powder was obtained. After the hydrolysis and condensation reactions, the possible structure of nanocomposites is as shown in Figure 9.

3.3. Photodegradation experiments

For the photocatalytic degradation experiment, the necessary volume of MG solution was added to the nTC. The prepared nTC/MG dye mixture was incubated in the dark for 90 min to equilibrate, the nTC/MG dye mixture was poured into a disposable flask, and the flask was quickly placed in the SOLARBOX, ready for irradiation to induce the photochemical reaction. The decomposition of MG was monitored by measuring the absorbency at 614 nm (λ_{max}) and degradation was quantified by detecting MG concentration (C) before, during, and after

irradiation. Photocatalytic activity of the nTC was compared with pure nano-TiO_2 and commercial chitosan (MW = 100,000–300,000) for degradation of MG under optimum catalysis conditions determined for the nTC.

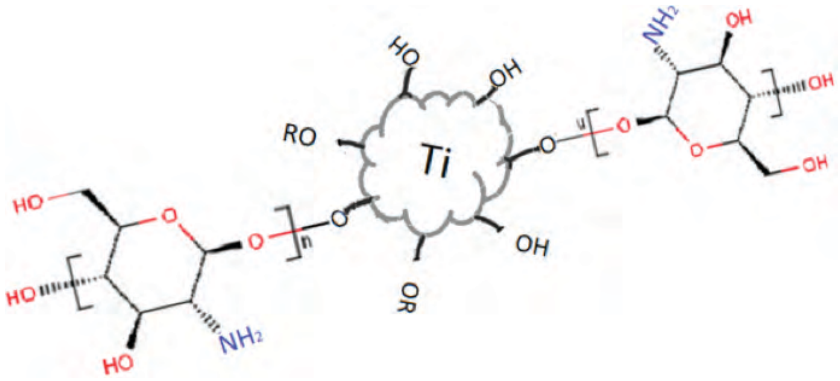

Figure 9. Schematic diagram of the possible structure of nTC.

References

1. Rinaudo, M. *Prog. Polym. Sci.* **2006**, *31*, 603–632.
2. Chatterjee, S.; Chatterjee, S.; Chatterjee, B. P.; Guh, A. K. *Process Biochem.* **2004**, *39*, 2229–2232.
3. Sudarshan, N. R; Hoover, D. G.; Knorr, D. *Food Biotechnol.* **1992**, *6*, 257–272.
4. Samar, M. M.; El-Kalyoubi, M. H.; Khalaf, M. M.; Abd El-Razik, M. M. *Ann. Agr. Sci.* **2013**, *58*, 33–41.
5. Pedroa, R. O., Takakia, M.; Gorayeb, T. C. C.; Bianchi, V. L. D.; Thomeo, J. C.; Tiera, M. J.; Tiera, V. A. O. *Microbiol. Res.* **2013**, *168*, 50–55.
6. Lehr, C. M.; Bouwstra, J. A.; Schacht, E. H.; Junginger, H. E. *Int. J. Pharm.* **1992**, *78*, 43–48.
7. Bagheri-Khoulenjani, S.; Taghizadeh, S. M.; Mirzadeh, H. *Carbohydr. Polym.* **2009**, *78*, 773–778.
8. Vaarum, K. M.; Myhr, M. M.; Hjerde, R. J. N.; Smidsroed, O. *Carbohydr Res.* **1997**, *299*, 99–101.
9. Vord, P. J. V.; Matthew, H. W. T.; DeSilva, S. P.; Mayton, L.; Wu, B.; Wooley, P. H. *J. Biomed. Mater. Res.* **2002**, *59*, 585–590.
10. Sashiwa, H.; Aiba, S. *Prog. Polym. Sci.* **2004**, *29*, 887–908.
11. Croisier, F.; Jérôme, C. *Eur. Polym. J.* **2013**, *49*, 780–792.
12. Palanisamy, B.; Babu, C. M.; Sundaravel, B.; Anandan, S.; Murugesan, V. *J. Hazard. Mater.* **2013**, *252–253*, 233–242.
13. Zhu, J. F.; Zhang, J. L.; Chen, F.; Anpo, M. *Mater. Lett.* **2005**, *59*, 3378–3381.
14. Ghezzar, M. R.; Abdelmalek, F.; Belhadj, M.; Benderdouche, N.; Addou, A. *J. Hazard. Mater.* **2009**, *164*, 1266–1274.
15. Addamo, M.; Bellardita, M.; Carriazo, D.; Paola, A. D.; Milioto, S.; Palmisano, L.; Rives, V. *Appl. Catal. B: Environ.* **2008**, *84*, 742–748.
16. Peller, J. R.; Whitman, R. L.; Griffith, S.; Harris, P.; Peller, C.; Scalzitti, J. *J. Photochem. Photobiol. A* **2007**, *186*, 212–217.
17. Berger, T.; Villarreal, T. L.; Satoca, D. M.; Gomez, R. *Electrochem. Commun.* **2006**, *8*, 1713–1718.
18. Anandan, S.; Vinu, A.; Venkatachalam, N.; Arabindoo, B.; Murugesan, V. *J. Mol. Catal. A: Chem.* **2006**, *256*, 312–320.
19. Lee, H. Y.; Kale, M. G. *Int. J. Appl. Ceram. Technol.* **2008**, *5*, 657–665.

20. Balachandaran, K.; Venckatesh, R.; Sivaraj, R. *Int. J. Eng. Sci. Tech.* **2010**, *2*, 3695–3700.
21. Bilton, M.; Milne, S. J.; Brown, P. A. *Open Journal of Inorganic Non-metallic Materials* **2012**, *2*, 1–10.
22. Ozerin, A. N.; Zelenetskii, A. N.; Akopova, T. A.; Pavlova-Verevkina, O. B.; Ozerin, L. A.; Surin, N. M., Kechek'yan, A. S. *Polym. Sci. Ser. A.* **2006**, *48*, 638–643.
23. Kim, T. Y.; Lee, Y. H.; Park, K. H.; Kim, S. J.; Cho, S. Y. *Res. Chem. Intermediat.* **2005**, *31*, 343–358.
24. Tao, Y.; Ye, L.; Pan, J.; Wang, Y.; Tang, B. *J. Hazard. Mater.* **2009**, *161*, 718–722.
25. Zubieta, C. E.; Messina, P. V.; Luengo, C.; Dennehy, M.; Pieroni, O.; Schulz, P. C. *J. Hazard. Mater.* **2008**, *152*, 765–777.
26. Zainal, Z.; Hui, L. K.; Hussein, M. Z.; Abdullah, A. H.; Hamadneh, I. R. *J. Hazard. Mater.* **2009**, *164*, 138–145.
27. Li, Q.; Su, H.; Tan, T. *Biochem. Eng. J.* **2008**, *38*, 212–218.
28. Nawi, M. A.; Sabar, S.; Jawad, A. H.; Ngah, W. S. W. *Biochem. Eng. J.* **2010**, *49*, 317–325.
29. Nawi, M. A.; Jawad, A. H.; Sabar, S.; Ngah, W. S. W. *Desalination* **2011**, *280*, 288–296.
30. Srivastava, S.; Sinha, R.; Roy, D. *Aquat. Toxicol.* **2004**, *66*, 319–329.
31. Culp, S. J.; Bealand, F. A. *J. Am. Coll. Toxicol.* **1996**, *15*, 219–238.
32. Akar, E.; Altinişik, A.; Seki, Y. *Ecol. Eng.* **2013**, *52*, 19–27.
33. Sayılkan, F.; Asiltürk, M.; Tatar, P.; Kiraz, N.; Arpaç, E.; Sayılkan, H. *J. Hazard. Mater.* **2007**, *148*, 735–744.
34. Sonawane, S. H.; Chaudhari, S. A.; Ghodke, S. A.; Parande, M. G.; Bhandari, V. M.; Michra, S.; Kulkarni, R. D. *Ultrason. Sonochem.* **2009**, *16*, 351–355.
35. Yang, D.; Li, J.; Jiang, Z.; Lu, L.; Chen, X. *Chem. Eng. Sci.* **2009**, *64*, 3130–3137.
36. Patterson, A. L. *Phys. Rev.* **1939**, *56*, 978–982.
37. Sayılkan, F.; Erdemoğlu, S.; Asiltürk, M.; Akarsu, M.; Şener, Ş.; Sayılkan, H.; Erdemoğlu, M.; Arpaç, E. *Mater. Res. Bull.* **2006**, *41*, 2276–2285.
38. Mano, J. F.; Koniarova, D.; Reis, R. L. *J. Mater. Sci.- Mater. Med.* **2003**, *14*, 127–135.
39. Tao, Y.; Pan, J.; Yan, S.; Tang, B.; Zhu, L. *Mater. Sci. Eng. B.* **2007**, *138*, 84–89.
40. Zhou, X. J.; Guo, W. Q.; Yang, S. S.; Zheng, H. S.; Ren, N. Q. *Bioresource Technol.* **2013**, *128*, 827–830.
41. Gao, G.; Zhang, A.; Zhang, M.; Chen, J.; Zhang, Q. *Chin. J. Catal.* **2008**, *29*, 426–430.
42. Ju, Y.; Yang, S.; Ding, Y.; Sun, C.; Zhang, A.; Wang, L. *J. Phys. Chem. A* **2008**, *112*, 11172–11177.
43. Liu, Y.; Ohko, Y.; Zhang, R.; Yang, Y.; Zhang, Z. *J. Hazard. Mater.* **2010**, *184*, 386–391.
44. Daneshvar, N.; Salari, D.; Khataee, A. R. *J. Photochem. Photobiol. A* **2003**, *157*, 111–116.
45. Lu, C.; Wu, Y.; Mai, F.; Chung, W.; Wu, C.; Lin, W.; Chen, C. *J. Mol. Catal. A: Chem.* **2009**, *310*, 159–165.
46. Rauf, M. A.; Ashraf, S. S. *Chem. Eng. J.* **2009**, *151*, 10–18.
47. Sakthivel, S.; Neppolian, B.; Shankar, M. V.; Arabindoo, B.; Palanichamy, M.; Murugesan, V. *Sol. Energ. Mat. Sol. C.* **2003**, *77*, 65–82.
48. Prado, A. G. S.; Costa, L. L. *J. Hazard. Mater.* **2009**, *169*, 297–301.